JOURNAL OF MATERIAL SCIENCE 29 (1994) 5095–5103

Analysis of the effects of substrate temperature, concentration of tin chloride and nature of dopants on the structural and electrical properties of sprayed SnO_2 films

A. MESSAD, J. BRUNEAUX, H. CACHET, M. FROMENT
UPR15 du CNRS "Physique des Liquides et Electrochimie", Université Pierre et Marie Curie, Tour 22, 4 Place Jussieu, 75252 Paris Cedex 05, France

The correlations between structural and electrical properties of sprayed SnO_2 films have been investigated as a function of substrate temperature (380–560 °C), concentration of tin precursor (0.02–0.8 M $SnCl_4$) and the nature of the doping agent (chlorine, fluorine, antimony). High-resolution transmission electron microscopy has shown that chlorine or fluorine incorporation promotes the same type of defects, which are ⟨0 1 1⟩ twins. These latter behave as neutral defects, the density of which limits the carrier mobility of degenerated fluorine- or chlorine-doped films to around 20 $cm^2 V^{-1} s^{-1}$. The situation is totally different with antimony. Below the solubility limit in the SnO_2 lattice (3%–4% Sb/Sn), Sn^{4+} are substituted by Sb^{5+}, creating two conduction electrons per site and acting as point-charged defects which lower carrier mobility. Above this limit, the Sb^{3+} and Sb^{5+} forms coexist and are associated with an extremely large concentration of structural defects, especially twins induced by the Sb^{3+} species. These ions enter two-dimensional arrangements on both sides of the twins, making them planar charged defects.

1. Introduction

Wide band-gap oxide films are extensively used in many applications such as sensors [1], photovoltaic [2–4], photoelectrochemical [5–7], and display devices [8], and for electrochemical engineering [9, 10]. Among the available materials, tin oxide (SnO_2) constitutes a good candidate because of its chemical stability and transparency. It can also be obtained as a resistive or a highly conductive material. One of the most commonly employed methods for preparing polycrystalline SnO_2 films is spray pyrolysis. In this technique, chemicals are brought to the pre-heated substrate surface as atomized droplets. Each one contains an amount of precursors (tin salt and other salts for doping), the concentration of each constituent being that in the sprayed solution. The pyrolysis reaction kinetics and the losses of chemicals by evaporation are strongly influenced by the substrate temperature. Although the role of this factor has been largely addressed in literature, the effect of concentration and the nature of precursors has been much less taken into consideration. Recently, the effects of tin incorporation into indium oxide films formed by plasma-assisted electron beam evaporation have been addressed [11]. For these films characterized by a low density of dislocations and stacking faults, it was suggested that tin not only acts as a donor but also contributes to decrease mobility by the creation of scattering centres. In this paper, we intend to examine the combined effect of the substrate temperature and the composition of the solution (both tin and doping salts) on the structural and electrical properties of SnO_2 films formed by spraying. In particular, we report the correlations between the structural defects, intrinsic or induced by the doping atoms, and the mobility of free carriers.

2. Experimental procedure

SnO_2 films were formed by spraying an $SnCl_4$ solution in methanol in the molar concentration range 0.1–0.8 M at a rate of 3 $cm^3 min^{-1}$. After degreasing and cleaning, the glass substrates (Pyrex) were heated at a set temperature between 380 and 560 °C. The carrier gas was air, supplied at a rate of 7 $dm^3 min^{-1}$. The deposition rate was estimated by measuring the thickness of the layers formed after different spraying times by means of an optical technique (Nomarsky differential interferometry [12]). Because of the precursor used, SnO_2 films always contain chlorine atoms which generate free carriers (unintentional doping). The presence of chlorine atoms was detected by Auger electron spectroscopy (AES) [13, 14]. A quantitative analysis was carried out by secondary ion mass spectroscopy (SIMS) indicating a strong concentration dependence upon the substrate temperature, T_{sub}, the ratio Cl/O being lower than 1% for $T_{sub} < 400$ °C

0022–2461 © *1994 Chapman & Hall*

[15]. In this work, the bulk chlorine concentration was determined by Rutherford back-scattering (RBS).

Intentional doping by fluorine or antimony was realized by adding NH_4F or $SbCl_3$ to the spray solution. RBS is unsuitable for determining a low fluorine content in the presence of a large amount of oxygen. In the literature, measurements of the F/O ratio in the range 1%–10% were performed by SIMS [15] and by a nuclear resonant reaction technique [16].

Resistivity and Hall measurements for conductive material were carried out by means of an a.c. technique associated with a square-wave modulation of the magnetic field and a lock-in detection. Structural characterizations by transmission electron microscopy (TEM) were achieved using a 100 kV (Jeol 100CX2) electron microscope and a 200 kV (Jeol 2000FX) apparatus for high-resolution transmission electron microscopy images (HRTEM). Thin SnO_2 films were prepared by using a technique described elsewhere [12]. Cross-sections were produced starting from SnO_2 films deposited on silicon substrates, the final thinning being realized by ion milling.

3. Influence of dopants and substrate temperature on growth conditions

The structural organization, especially the formation of defects, is expected to depend on the growth rate of the deposit. Fig. 1 shows the variations of the deposition rate (in the range 0.5–5 nm s^{-1}) against the reciprocal substrate temperature for unintentionally doped films. From this semilogarithmic plot, two regimes can be distinguished, roughly above or below $T_{sub} \simeq 500\,^{\circ}C$. Below this temperature, the deposition rate is activated with T_{sub} and increases with C_{Sn}, the molar tin salt concentration, suggesting that the precursors would be in a liquid phase. An heterogeneous

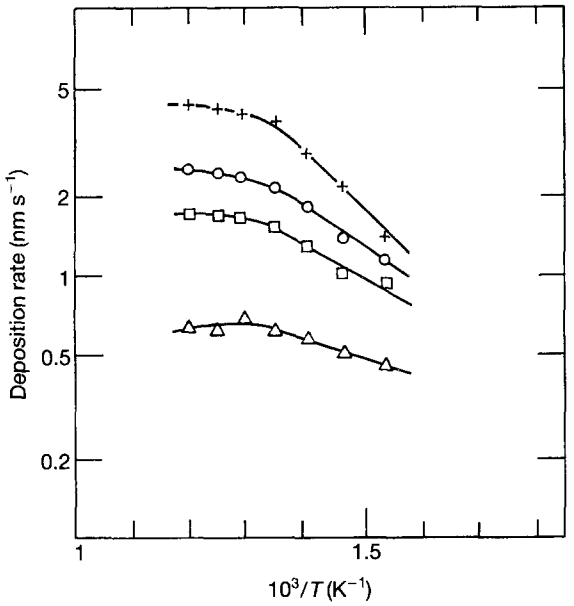

Figure 1 Deposition rate of sprayed undoped SnO_2 films plotted against reciprocal temperature at different $SnCl_4$ concentrations showing the existence of two deposition regimes. Concentration: (+) 0.8 M, (○) 0.5 M, (□) 0.2 M, (△) 0.1 M.

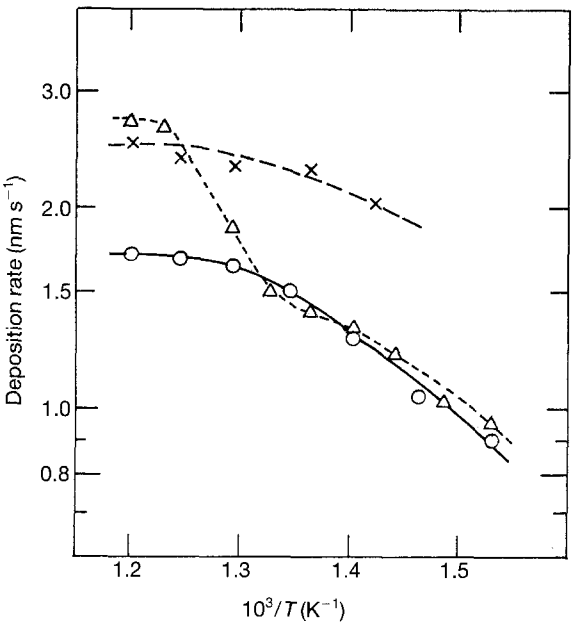

Figure 2 Deposition rate plotted against reciprocal temperature as a function of the nature of the dopant: (○) undoped, (△) fluorine-doped, (×) antimony-doped.

reaction would take place between the reactive species transported in the liquid phase and the solid substrate. At a temperature higher than 500 °C, the deposition rate does not depend very much on T_{sub}: a quasi-plateau is observed, the amplitude of which is found to be proportional to C_{Sn}. In this temperature range, the evaporation of the solvent is achieved. The precursors are in the vapour state and the growth mechanism is analogous to a chemical vapour deposition (CVD) process ([17] and references therein). The efficiency of our spray arrangement was around 5%–25%, the best values being obtained for $C_{Sn} = 0.2$–0.3 M and $T_{sub} > 500\,^{\circ}C$.

Fig. 2 shows how much the growth rate is influenced by the type of doping. The unintentionally doped and antimony-doped films present a similar behaviour characterized by two regimes (control by kinetics or by mass transport) as discussed above. But the growth rate is twice as fast in the presence of antimony, the efficiency approaching 50%. With fluorine, as long as T_{sub} is lower than 500 °C, the growth rate is very close to that for the undoped material. For T_{sub} above 500 °C, the deposition rate sharply increases and becomes larger than that observed for antimony-doped films. This behaviour can be correlated with the chlorine content in the film, which is known to decrease when T_{sub} increases and to be negligible above 500 °C [15]. The reduced growth rate might be related to the incorporation process of foreign atoms into the SnO_2 lattice, slower for chlorine because of more evaporation than for fluorine or antimony (see Section 4.2).

4. Unintentionally doped and fluorine-doped films

4.1. Unintentionally doped films

Fig. 3 shows the evolution of the SnO_2 structure with the $SnCl_4$ concentration, C_{Sn}, and the substrate tem-

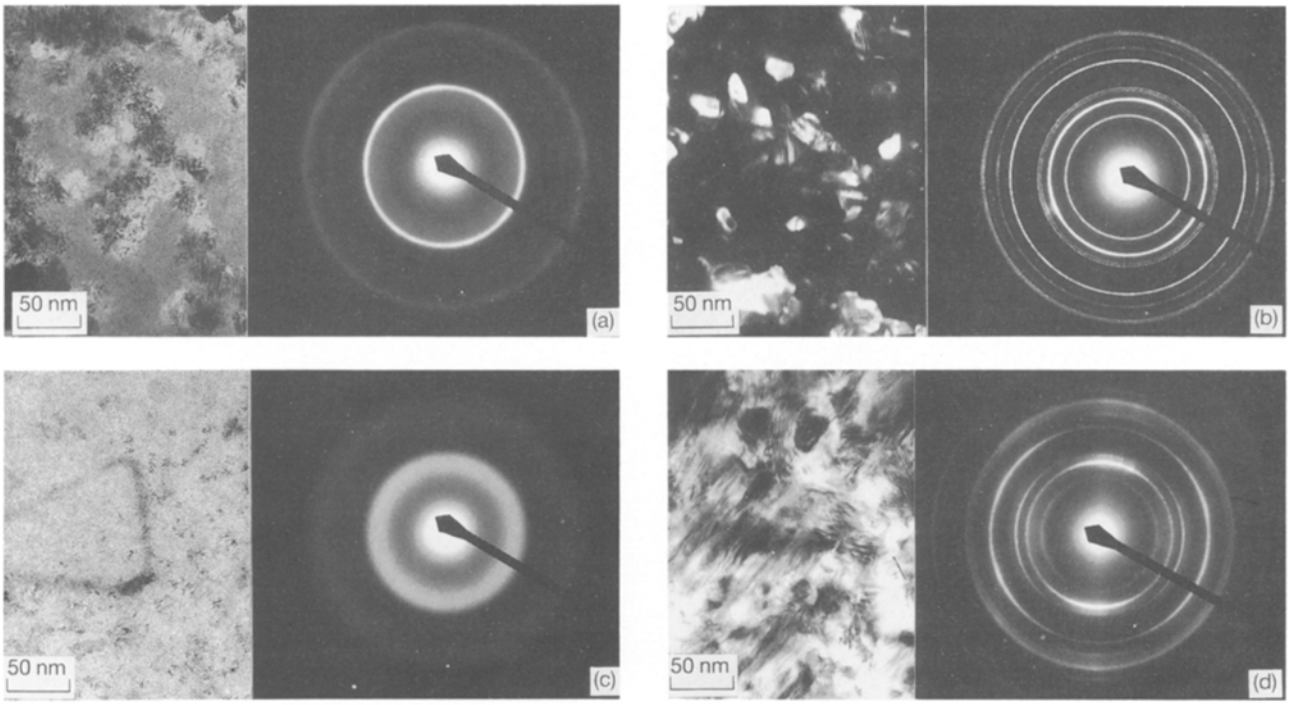

Figure 3 TEM images and microdiffraction patterns of SnO_2 films prepared at different $SnCl_4$ concentrations and substrate temperatures. (a) 0.1 M, 380 °C; (b) 0.1 M, 560 °C; (c) 0.8 M, 380 °C; (d) 0.8 M, 560 °C.

perature, T_{sub}, as determined by TEM images and microdiffraction patterns. The films formed at a low temperature (below 400 °C) or at a very large C_{Sn} concentration (i.e. 0.8 M) tend to be amorphous. It should be noted that the higher the substrate temperature, the better the crystallinity of the films, in agreement with previous observations [12, 18]. Additionally, HRTEM examination of film cross-sections shows the absence of preferential orientation at T_{sub} = 400 °C (Fig. 4a) and the formation of a columnar grain structure along the ⟨1 0 0⟩ axis at 500 °C (Fig. 4b) in accordance with previous conclusions given in the literature [19, 20]. Fig. 5 shows an HRTEM view of ⟨0 1 1⟩ SnO_2 twins. This image reveals that in the concentration range considered for C_{Sn}, the dominant structural defects are such planar defects, the linear density of which is relatively high, about 10^7–10^8 m^{-1}. The variations of the mean grain size with T_{sub} and C_{Sn}, as deduced from transmission electron micrographs, are illustrated in Fig. 6. At a fixed C_{Sn}, the grain size increases linearly with T_{sub}. Such behaviour can be understood as follows. When T_{sub} is increased, the atoms arriving at the surface are able to diffuse and reach the nuclei which are already growing. This process tends to limit the density of nuclei and then promotes the increase in grain size. On the contrary, if T_{sub} is lowered, or C_{Sn} is very high, the density of nuclei becomes so large that the grain size is kept small and an amorphous material is found. From the data in Fig. 6, it is deduced that, at a given

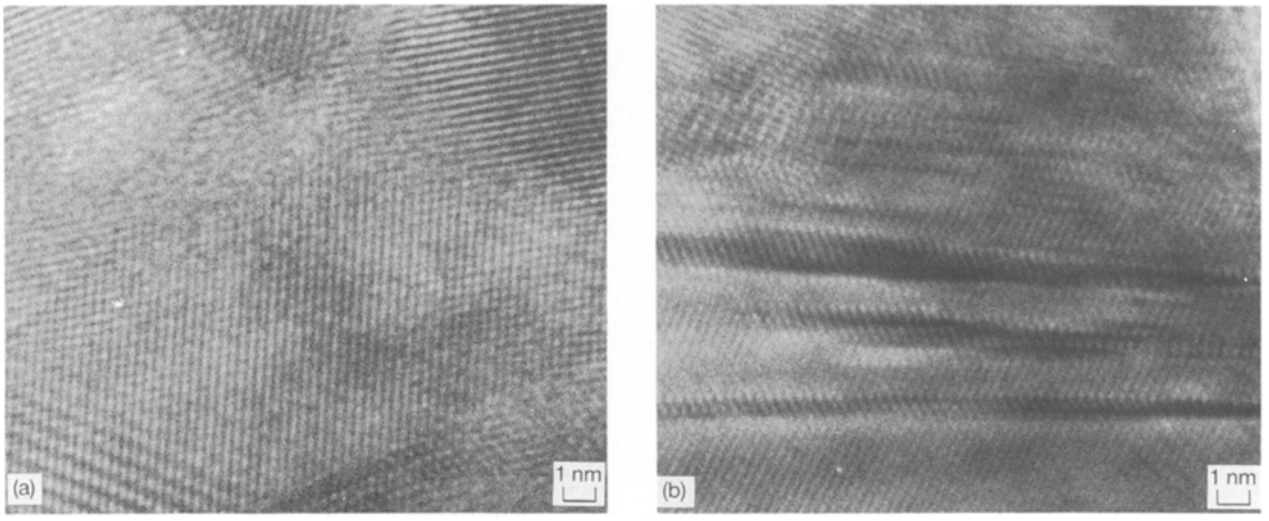

Figure 4 HRTEM cross-sections of SnO_2 films: (a) substrate temperature 400 °C; (b) substrate temperature 500 °C.

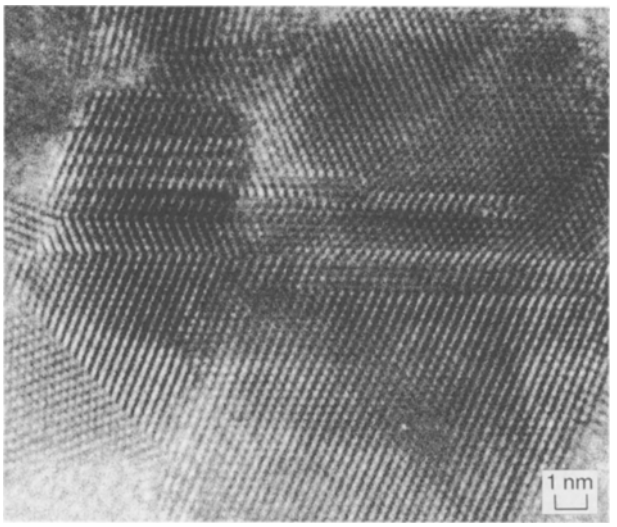

Figure 5 HRTEM view of ⟨0 1 1⟩ twins in an SnO_2 film (0.002 M $SnCl_4$ + 0.000 14 M NH_4F; substrate temperature = 500 °C).

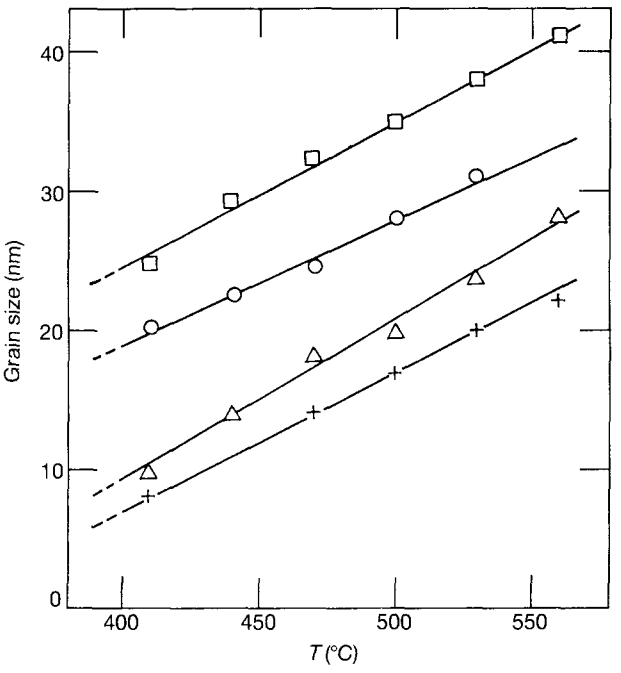

Figure 6 Dependence of grain size on the substrate temperature for different $SnCl_4$ concentrations: (+) 0.8 M, (○) 0.5 M, (□) 0.2 M, (△) 0.1 M.

temperature, the grain size presents a maximum for C_{Sn} between 0.2 and 0.5 M.

Fig. 7a shows the dependence of the carrier concentration upon the substrate temperature at a set $SnCl_4$ concentration. In a general way, the carrier concentration increases with T_{sub}, reaching a "flat" maximum and then decreasing by an order of magnitude: the higher the tin salt concentration, C_{Sn}, in the spray solution, the higher is the temperature at which the carrier concentration is maximum. In order to address the actual role of the incorporated chlorine atoms with respect to the electrical properties, RBS analysis has been performed to allow the chloride concentration, N_{Cl}, to be determined. The results are gathered in Table I. Because of the very small amplitude of the

TABLE I Chloride ion concentration, N_{Cl^-}, as determined by RBS and density, N, from Hall measurements for unintentionally doped SnO_2 films

[Sn] (mol l^{-1})	T (°C)	N (cm^{-3})	N_{Cl^-} (cm^{-3})
0.1	410	1.3×10^{20}	3.3×10^{20}
	440	1.0×10^{20}	1.0×10^{20}
	560	1.3×10^{19}	–
0.2	410	1.3×10^{20}	–
	440	1.3×10^{20}	–
	560	3.8×10^{19}	–
0.5	410	8.9×10^{19}	2.3×10^{20}
	470	1.7×10^{20}	1.2×10^{20}
	560	5×10^{19}	1.1×10^{20}
0.8	410	5.2×10^{19}	1.4×10^{21}
	500	1.1×10^{20}	2.1×10^{20}
	560	1.0×10^{20}	2.1×10^{20}

chlorine peak compared to the signal-to-noise ratio, the precision for N_{Cl} lies in between 20% and 50%. Nevertheless, from Table I, it can be concluded that, for a given C_{Sn}, N_{Cl} decreases when T_{sub} is increased. This behaviour is in agreement with previous observations based on AES [14, 21] or SIMS experiments [15]. For the films formed with a C_{Sn} = 0.1 M solution, the carrier density can be identified with the chlorine content. This supports the "valence-controlled" semiconductor model in which it is assumed that δ Cl^- ions substitute δ O^{2-} ions leading to δ-free electrons (originating from the 5 *s* orbital of the tin atoms) per SnO_2 molecules [22]. The same remark applies to the films formed with the more concentrated solutions (0.5 and 0.8 M) except at the lowest temperature examined (410 °C) for the 0.8 M solution. In this latter case, the large difference between N_{Cl} and the carrier density may be attributed to the amorphous character of the material promoting the incorporation of chlorine atoms without bond-breaking generating conduction electrons [23]. The variations of the mobility and resistivity with T_{sub} are given in Fig. 7b and c, respectively. Mobility (resistivity) exhibits a maximum (minimum) when T_{sub} is increased: the higher is C_{Sn} in the spray solution, the higher is the temperature corresponding to the extremum. The temperature dependence of the resistivity is in agreement with previous data in the literature [14, 19, 24]. Note that the change in resistivity is essentially governed by the change in carrier density. Mobility does not change as much. It depends on the crystalline quality. The improvement of the mobility when increasing T_{sub} would be due to the larger grain size [24] and the better crystallinity within the grain (Fig. 3). The mobility drop occurring at higher temperature might be attributed to a loss of cohesion between adjacent grains because of an enhanced deposition rate.

4.2. Fluorine-doped films

Fluorine is one of the most commonly used doping agents for SnO_2. It is readily incorporated by adding NH_4F to the spray solution. In this way, it is possible to gain one order of magnitude for the film resistivity

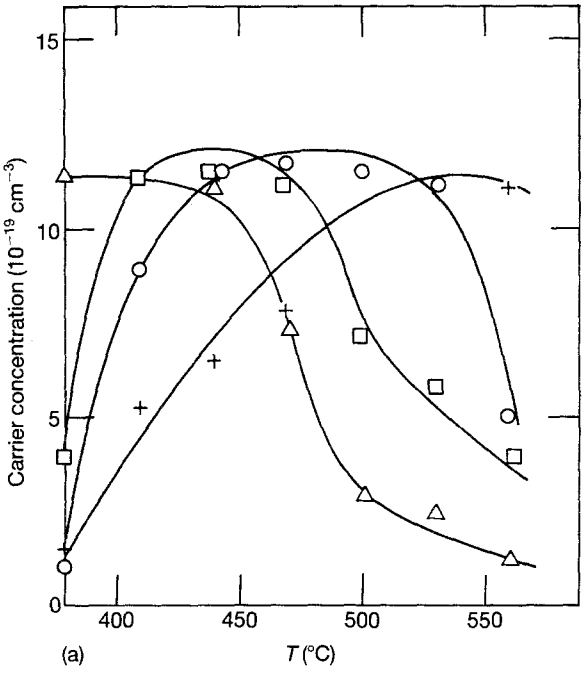

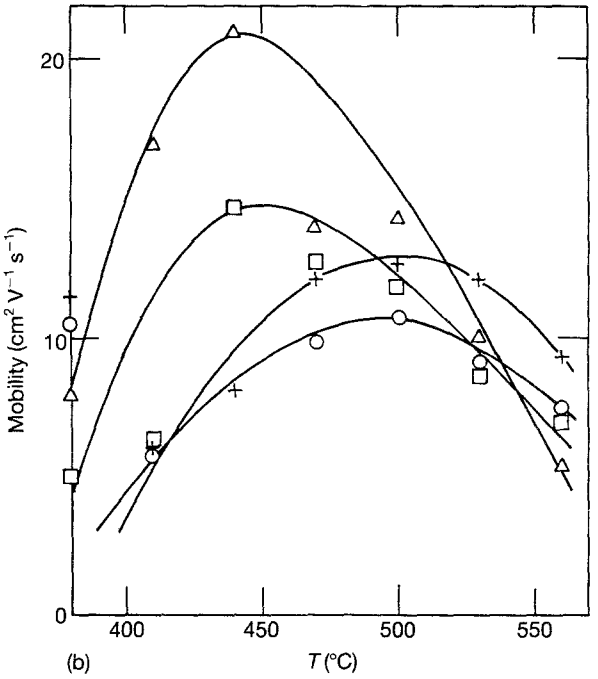

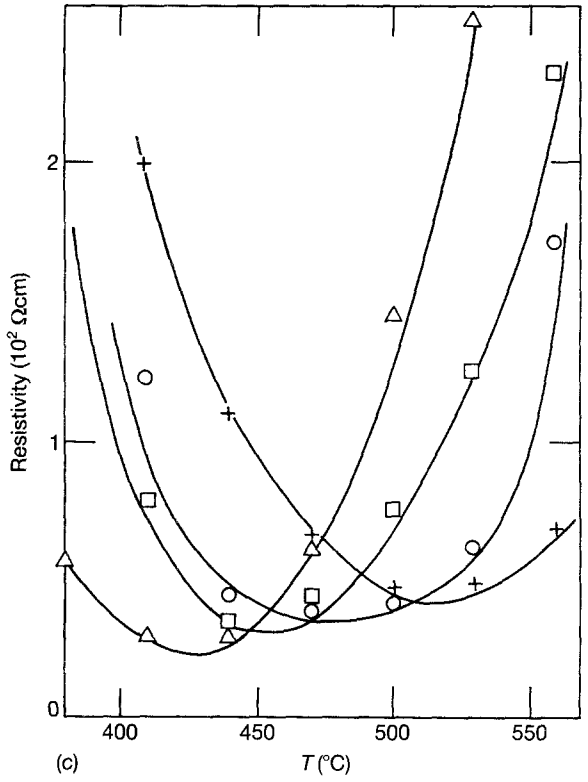

Figure 7 Influence of the substrate temperature and $SnCl_4$ concentration on (a) the carrier density, (b) the carrier mobility and (c) the resistivity of sprayed undoped SnO_2 films. For key, see Fig. 6.

compared to the doping by chlorine only [13, 25]. From a mechanistic point of view, the incorporation of a fluorine atom resembles that of a chlorine one, but it is easier because of the lower ionic radius of F^- (0.133 nm for F^- instead of 0.181 nm for Cl^- [26]) comparable to that of O^{2-} (0.132 nm). A direct consequence is that the SnO_2 lattice is able to incorporate many more F^- ions than Cl^- ions and then to generate a larger density of carriers. SIMS measurements have shown that fluorine is incorporated within a few per cent for T_{sub} around 400 °C whereas the chlorine content strongly decreases below 1% with T_{sub} because of evaporation [13, 15].

5. Antimony-doped films

Antimony-doping of SnO_2 is realized by the addition of $SbCl_3$ in the spray solution. At low concentration, antimony can substitute tin atoms as Sb^{5+} in the SnO_2 lattice according to the reaction scheme: $Sb^{3+} \rightarrow Sb^{5+} + 2e^-$ [27]. During growth, the lone pair of Sb^{3+} plays a stereochemical role similar to that of O^{2-} or F^- [28]: it is able to occupy an atomic site in the lattice, replacing one oxygen atom. The incorporation of antimony as a Sb^{5+} ion is then equivalent to the formation of one neutral oxygen vacancy and two conduction electrons. When the antimony content is increased above a few per cent, depending on the film growth conditions, both Sb^{5+} and Sb^{3+} species coexist. A striking point is that Sb^{3+} ions are not able to satisfy any coordination sites in the SnO_2 lattice and then induce new geometric and electrical defects. As proved by TEM observations in Fig. 8b, antimony-doped SnO_2 films are characterized by an extremely large concentration of structural defects, especially twins, compared to the undoped films (Fig. 8a). The mean distance between two twin planes is around 1 nm. Sb^{3+} cannot satisfy the octahedral coordination of Sn^{4+} and Sb^{5+}, but may fit a bipyramidal–trigonal coordination [29], as shown in Fig. 9. Accordingly, SbO_4 cages may be formed during the film growth, leading to the emergence of twins.

Fig. 10 represents the variations of carrier density and resistivity against the relative concentration Sb/Sn in the spray solution, for two series of films corresponding to a 0.02 M or 0.2 M $SnCl_4$ concentration, respectively. In both cases, a minimum of resistivity is observed which is often considered as an indication of the limit of solubility of Sb^{5+} in the SnO_2 lattice [27]. This limit would be between 1%

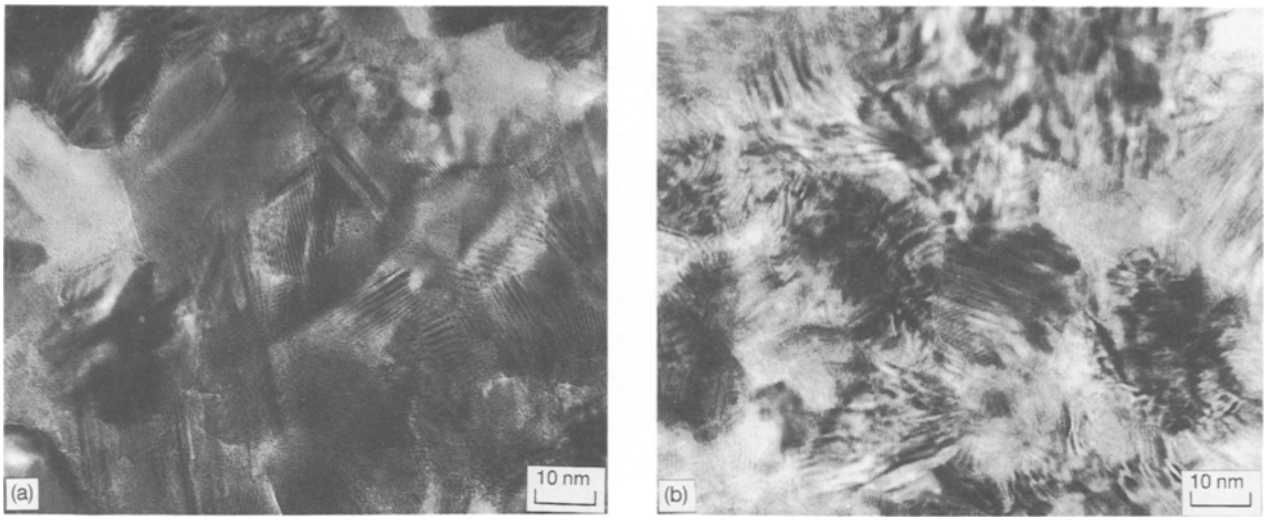

Figure 8 TEM image of (a) undoped, (b) antimony-doped SnO_2 films showing the large increase in defect density induced by the antimony doping.

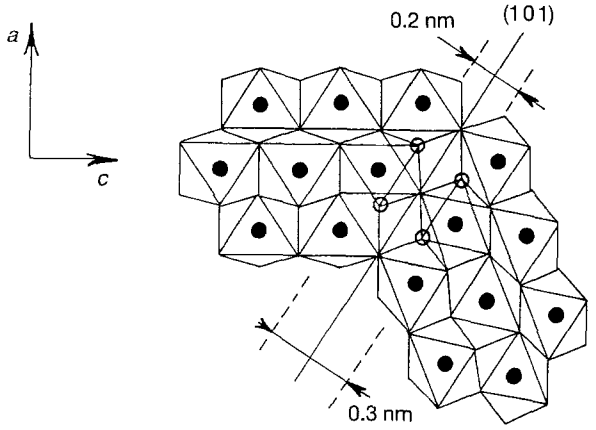

Figure 9 Structural arrangement of antimony-doped SnO_2 in the presence of a twin showing the (○) Sb^{3+} and (●) Sn^{4+} sites adjacent to the twin boundary. For SnO_2, $a = b = 0.4737$ nm and $c = 0.3180$ nm.

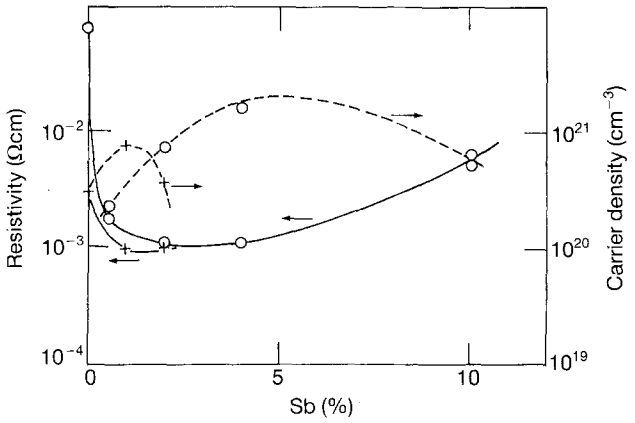

Figure 10 Resistivity and carrier density of antimony-doped SnO_2 films formed at 500 °C, for two $SnCl_4$ concentrations: (○) 0.002 M; (+) 0.2 M. The antimony concentration is given as the ratio Sb/Sn (%) in solution.

and 2% (2% and 4%) for the films produced from a 0.2 M (0.02 M) $SnCl_4$ solution. Starting from the maximum of the carrier density and subtracting the contribution of Cl^- ions leads to a better defined estimation: 1.2% (3.6%), respectively. This latter value is comparable to those found by other authors from conductivity measurements, 5% [30] and 3% [31]. The difference in the solubility limit between the two series of films might be attributed to the difference in growth rate, around ten times smaller with the more dilute $SnCl_4$ solution (see Section 3).

From the above discussion, we can assume that (i) below the solubility limit, antimony is dispersed in the SnO_2 matrix as Sb^{5+} species which act as ionized impurities, (ii) above the solubility limit, antimony is

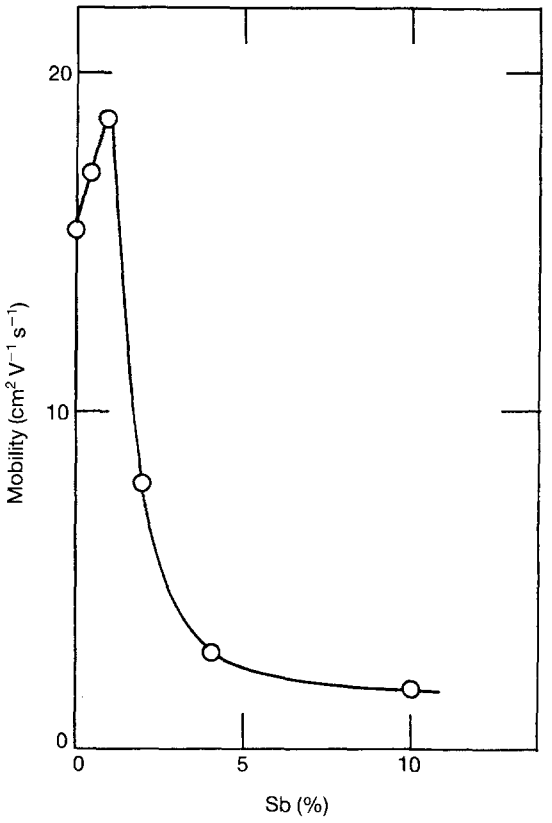

Figure 11 Mobility as a function of the antimony concentration (expressed in Sb/Sn at %) for antimony-doped sprayed SnO_2 films formed at 500 °C from a 0.02 M $SnCl_4$ solution.

also incorporated as Sb^{3+} which segregate towards twin regions to form electrically charged planar defects. To ascertain the actual role of antimony upon the electrical properties of SnO_2:Sb films, we compared the experimentally determined mobility with some theoretical models as a function of the antimony content. The mobility data have been obtained for SnO_2 films formed at 500 °C with $0 < Sb/Sn < 0.1$, from a 0.02 M $SnCl_4$ solution (Fig. 11). Such a dilute solution has been preferentially chosen because it is known from previous studies [25] that the density of crystallographic defects (twins) is strongly reduced by comparison with the case of concentrated solutions. In Fig. 11, the mobility presents a sharp peak around 1%, followed by an abrupt decrease and, above 5%, the beginning of a plateau. Such a behaviour is in agreement with the data of Shanthi *et al.* [24]. These authors tentatively explained their mobility data by considering the contribution of two scattering mechanisms: (i) grain-boundary scattering, (ii) ionized impurity scattering. The first mechanism was proved to account well for the mobility data of undoped SnO_2 films. The second one was expected to be dominant at large antimony concentration yielding to a decrease in mobility. The increase in mobility observed at low antimony content was qualitatively attributed to a decrease of the grain-boundary scattering because of an increase in the grain size. The dependence of the mobility on the antimony concentration, taking into account the different possibilities to incorporate antimony ions into the SnO_2 lattice, is considered in more detail below.

At zero antimony content, the carrier concentration is as low as $\approx 5 \times 10^{18}$ cm^{-3}; we have demonstrated previously that mobility is mainly governed by the barrier effect of grain boundaries which act as electrical traps [25]. Under these conditions, grains are partially depleted and the mobility value is strongly reduced. It may drop to a nearly zero value when the grains are fully depleted. The major effect of the presence of small quantities of antimony is then to increase the number of free carriers up to $\approx 10^{20}$ cm^{-3}. Grains are less and less depleted; mobility increases and tends to be essentially limited by the bulk properties of the grains. The decrease in mobility beyond 1% Sb (Fig. 11) suggests that carrier diffusion by ionized antimony impurities becomes dominant. The effect of this mechanism is analysed on the basis of a relatively simple model, the details of which are given in Appendix 1. In this model, it is assumed that carriers constitute a degenerate electron gas moving through a dielectric medium containing a distribution of diffusion centres represented by $(+ze)$ charged points. Mobility is calculated by considering that the heat produced by the Joule effect is equal to the energy loss of electrons [32]. According to the theoretical expression for the mobility (Equation 4), calculations were carried out by taking a fixed value for the dielectric constant $\varepsilon = 10$ [33] and for $z = +3$ and $z = +5$. The results are presented in Table II. The agreement between theory and experiment was obtained by fitting the effective mass, m^*/m_0. The assumption $z = +3$ leads to unacceptable m^*/m_0 values, either larger than unity or larger than the literature data for antimony-doped SnO_2 films corresponding to $N < 10^{21}$ cm^{-3} [34]. On the other hand, considering $z = +5$, the calculated values agree satisfactorily with the existing data ($0.2 < m^*/m_0 < 0.35$ for $N < 10^{21}$ cm^{-3}). The calculated effective mass increases with the carrier concentration from 0.24 (0.5% Sb) up to 0.64 (5% Sb), in agreement with the general tendency illustrated in Fig. 5 of [34] for fluorine- and antimony-doped films. At 10% Sb content, the calculated effective mass (0.27) is lower than the values for the lower antimony contents. This rather unexpected result suggests that above 5%, another diffusion mechanism by antimony has to be taken into account.

Beyond the limit of solubility of the Sb^{5+} ions, it has been stressed that Sb^{3+} species are also incorporated through the formation of twins. These planar defects are charged and give rise to a potential barrier. Depending on the barrier width, carriers can flow through by tunnelling. On the basis of the transmission electron micrographs (see Fig. 8), the actual situation can be approached by the one-dimensional model described in Appendix 2. Charged twins (thickness w, density of Sb^{3+} in the twin region N_{Sb}) are assumed regularly spaced with a linear density, L^{-1}. Equation A5 gives the full expression for the resistivity, ρ, as a function of w, N_{Sb}, L, m^* the effective mass of electrons and N the carrier density. Calculations were performed for the 10% Sb/Sn sample using the following experimental values: $\rho = 5.5 \times 10^{-3}\ \Omega$ cm and $N = 6 \times 10^{20}$ cm^{-3}. The problem is to obtain an estimation of N_{sb}, i.e. the concentration of Sb^{3+} ions. Up to 4%–5% Sb/Sn, antimony is essentially incorp-

TABLE II At each antimony concentration, the effective mass, m^*/m_0, is adjusted to make the calculated mobility (according to Equation A4) to be equal to the measured one

Sb (%) in solution	N_{Sb} (10^{20} cm^{-3}) in SnO_2	N (10^{20} cm^{-3}) (Hall)	μ (cm^2 V^{-1} s^{-1})	Calculated effective mass, m^*/m_0	
				$Z = 5$	$Z = 3$
0	0		15.0		
0.5	1.0	2.1	17.0	0.24	0.49
1.0	1.4	2.7	18.5	0.22	0.44
2.0	3.8	7.5	7.9	0.34	0.69
3.0	6.8	13.5	4.0	0.50	(1.04)
4.0	9.5	19.0	2.8	0.60	(1.28)
5.0	10.5	21.0	2.5	0.64	(1.36)
10	21	6.0	1.9	0.27	0.54

orated as Sb^{5+} and the carrier concentration, N, is twice the concentration of Sb^{5+}. Within experimental uncertainty, Hall measurement data show that N is proportional to the antimony concentration in the spray solution (see Table II). This demonstrates that, at least up to 5% Sb/Sn, the amount of antimony incorporated into the film is proportional to the antimony concentration in solution. If we assume that it is also true for Sb/Sn = 10%, the extrapolated concentration of antimony atoms incorporated into SnO_2 would be $\approx 2.1 \times 10^{21}\ cm^{-3}$. Subtracting the concentration of Sb^{5+} ($= 3 \times 10^{20}\ cm^{-3}$ from the measured Hall carrier density), we obtain the concentration of Sb^{3+} as $N_{Sb} = 1.8 \times 10^{21}\ cm^{-3}$. The effective mass was extrapolated from the data of Table II and taken as $m^* = 0.643$. By injecting trial values for w, L is calculated and compared to the experimental mean value estimated from the TEM observations. A good compromise is obtained for $w \approx 0.2$ nm yielding $L^{-1} \approx 10^9\ m^{-1}$. Note that $w = 0.2$ nm (0.3 nm) corresponds to the distance between two Sb^{3+} (Sn^{4+}) ions on both sides of the planar defect, as depicted in Fig. 9. This figure shows the SnO_2 lattice with a (1 0 1) twin boundary (oxygen plane) across. The case $w = 0.3$ nm is unlikely, because antimony cannot substitute tin without perturbing the lattice. Instead of the octahedral coordination of Sn^{4+}, Sb^{3+} accommodates to a bipyramidal trigonal coordination which gives rise to the formation of twins (Fig. 9).

6. Discussion and conclusion

Fig. 12 gives a comparison between the three different types of doping with respect to some electrical properties of SnO_2 films formed from a 0.2 M $SnCl_4$ solution. The lowest resistivity and the highest mobility are obtained for the fluorine-doped films for which carrier density and mobility are simultaneously maximized.

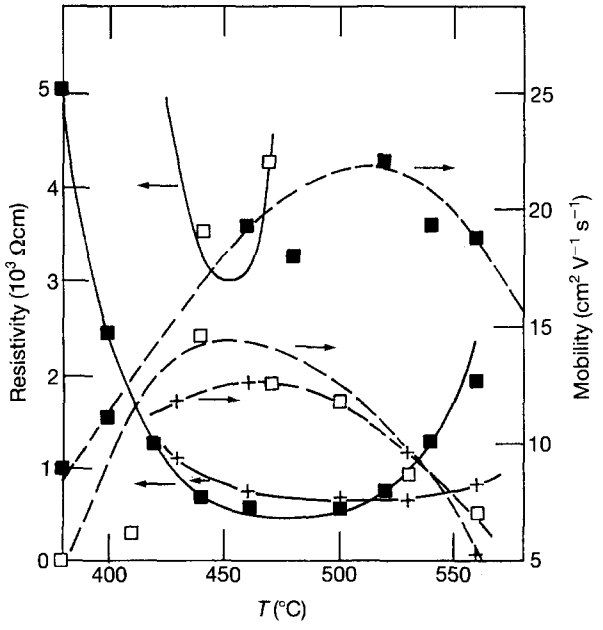

Figure 12 Effect of the nature of the dopant on the resistivity and mobility of SnO_2 films formed from a 0.2 M $SnCl_4$ solution as a function of the substrate temperature: (□) undoped; (■) fluorine-doped (F/Sn = 70%); (+) antimony-doped (Sb/Sn = 4%).

This is not the case for the antimony-doped film: the low resistivity is achieved owing to a very large number of carriers, but their mobility is reduced by the high density of electrical and structural defects (see Fig. 8). If we compare F^- and Cl^- doping, note that both species generate the same type of structural defects: during the film growth, the incorporation of F^- or Cl^- ions promotes the formation of the same type of twins (0 1 1) by substituting O^{2-} ions. The twin boundary corresponds to a ⟨0 1 1⟩ tin plane. Consequently, with chlorine or fluorine as dopant, the twins which are formed do not disturb the continuity of the SnO_2 lattice and behave as neutral defects. Such defects are responsible for the relatively low mobility values (around $20\ cm^2 V^{-1} s^{-1}$) obtained for the conductive tin oxide films [25], the better results with F^- being probably due to its smaller carrier diffusion cross-section compared to that of Cl^-. The situation is totally different with antimony. At low concentration, antimony is incorporated as Sb^{5+} replacing Sn^{4+} ions and is randomly distributed in the lattice. Sb^{5+} sites behave as point-charged defects. Increasing the antimony concentration beyond the solubility limit leads to the coexistence of both Sb^{5+} and Sb^{3+} species. The coordination of Sb^{3+} implies the formation of twins with an oxygen plane as twin boundary. Sb^{3+} ions segregate in the twin region which is equivalent to a planar-charged defect.

From the present study, it can be concluded that the transport properties of sprayed SnO_2 films are strongly influenced by the crystallographic defects generated by the dopants but in different ways: fluorine and chlorine promote neutral structural defects whereas antimony gives rise to point- or planar-charged defects depending on the quantity incorporated.

Appendix 1. Diffusion of carriers by charged impurities

We consider a degenerated electron gas flowing through a dispersed medium of charged diffusion centres, i.e. Sb^{5+} ions. These centres occupy fixed positions in the lattice. It is assumed that the loss of electron energy per unit of time, dW/dt, due to diffusion is equal to the power produced by the Joule effect [35]

$$N_i \frac{dW}{dt} = \boldsymbol{JE}$$

$$\boldsymbol{JE} = \rho |\boldsymbol{J}|^2$$

$$|\boldsymbol{J}|^2 = |Ne\boldsymbol{v}|^2 \qquad \text{(A1)}$$

where N_i is the density of diffusion centres, N the electron concentration, $\boldsymbol{v}$ the electron velocity, e the elementary charge, $\boldsymbol{J}$ the electron current with $\boldsymbol{J} = Ne\boldsymbol{v}$, and $\boldsymbol{E}$ the electric field.

The energy loss depends on the charge, Ze, of the diffusion centre, the electron velocity, v, and the dielectric function of the material, $\varepsilon(\boldsymbol{k}, \omega)$ [36]. This latter depends on the excitation frequency, ω, and the wave vector, $\boldsymbol{k}$. The loss of energy per unit of time is given by

$$-\frac{dW}{dt} = -\frac{Z^2 e^2}{(2\pi)^3 \varepsilon_0} \int d^3k \frac{\boldsymbol{kv}}{k^2} \mathrm{Im}\left[\frac{1}{\varepsilon(\boldsymbol{k}, \omega)}\right] \qquad \text{(A2)}$$

where Im stands for the imaginary part and $\varepsilon_0 = 8.84 \times 10^{-12}\ \mathrm{F\,m^{-1}}$. For a degenerate gas, the imaginary and real parts of $\varepsilon(\boldsymbol{k}, \omega)$ are given by Pines [36]. The low-frequency limit ($\omega = 0$) yields the static resistivity and mobility, μ

$$\rho = \frac{N_i Z^2 e^2 m^{*2}}{24\pi^3(\varepsilon_0\varepsilon)^2\hbar^3 N^2}\bar{f}(p') \tag{A3}$$

$$\mu = \frac{1}{N\rho e} \tag{A4a}$$

with

$$\bar{f}(p') = \ln(1 + p'^2) - [p'^2/(1 + p'^2)] \tag{A4b}$$

$$p' = \frac{2k_F}{k_{FT}} \tag{A4c}$$

$k_F = (3\pi^2 N)^{1/3}$ the Fermi wave vector (A4d)

$$k_{FT}^2 = \left(\frac{3N}{\pi^4}\right)^{1/3}\frac{m^* e^2}{\varepsilon\varepsilon_0\hbar^2}$$

the Thomas–Fermi screening parameter (A4e)

where m^* is the effective mass of electrons, and ε the static dielectric constant.

Appendix 2. Model for twin boundaries charged with Sb^{3+}

A one-dimensional model is considered. Electrons are assumed to tunnel through electrical barriers formed by twins and regularly spaced by a distance L. The linear density of twins is then L^{-1}. The width, w, of each barrier is defined by the twin region containing Sb^{3+} ions located at favourable sites on both sides of the twin boundary. The resistivity due to the tunnelling process is then expressed by [37]

$$\rho = \frac{\hbar^3}{4\pi m^* e^2 L\xi}\exp\left[2\left(\frac{2m^*\varphi}{\hbar^2}\right)^{1/2} w\right] \tag{A5a}$$

with

$$\xi = \frac{\hbar^2}{2m^*}(3\pi^2 N)^{2/3} \tag{A5b}$$

the distance between the Fermi level and the bottom of the conduction band, and

$$\varphi = \frac{e^2 Q_t^2}{8\varepsilon\varepsilon_0 N} \tag{A5c}$$

the electrostatic potential barrier created by the surface charge density $Q_t = 3N_{Sb}w$, where N_{Sb} is the density of Sb^{3+} in the twin region.

References

1. Y. K. FANG, F. Y. CHEN, J. D. HWANG, B. C. FANG and J. R. CHEN, *Appl. Phys. Lett.* **62** (1993) 490.
2. T. FENG, A. K. GHOSH and C. FISHMAN, *ibid.* **35** (1979) 266.
3. A. SUBRAHMANYAM, V. VASU, P. SANTANARAGHAVAN, J. KUMAR and P. RAMASAMY, *Mater. Sci. Eng.* **B14** (1992) 365.
4. H. CACHET, A. MESSAD, M. FROMENT and J. BRUNEAUX, in "Optical Materials Technology for Energy Efficiency and Solar Energy Conversion XI: Photovoltaics, Photochemistry and Photoelectrochemistry", edited by A. Hugot, C. G. Granqvist, C. M. Lampert, *Proc. SPIE* 1729 (1992) p. 114.
5. F. DECKER, M. FRACASTORO-DECKER, W. BADAWY, K. DOBLHOFER and H. GERISCHER, *J. Electrochem. Soc.* **130** (1983) 2173.
6. J. BRUNEAUX, H. CACHET, M. FROMENT and A. MESSAD, *Electrochim. Acta* **36** (1991) 1787.
7. S. I. HO, D. P. WHELAN, K. RAJESHWAR, A. WEISS, M. MURLEY and R. REID, *J. Electrochem. Soc.* **135** (1988) 1452.
8. N. R. LYNAM, in "Proceedings of the symposium on Electrochromic Materials", edited by M. K. Carpenter and D. A. Corrigan, The Electrochemical Society, Proceedings Vol. 90–2 (1990) p. 201.
9. R. KÖTZ, S. STUCKI and B. CARCER, *J. Appl. Electrochem.* **21** (1991) 14.
10. CH. COMMNINELLIS and C. PULGARIN, *ibid.* **23** (1993) 108.
11. Y. SHIGESATO and D. C. PAINE, *Appl. Phys. Lett.* **62** (1993) 1268.
12. J. BRUNEAUX, H. CACHET, M. FROMENT, M. LEVART and J. VEDEL, *J. Microsc. Spectrosc. Electron.* **14** (1989) 1.
13. B. GOTTLIEB, R. KOROPECKI, R. ARCE, R. CRISALLE and J. FERRON, *Thin Solid Films* **199** (1991) 13.
14. K. H. KIM and C. G. PARK, *J. Electrochem. Soc.* **138** (1991) 2408.
15. J. FERRON and R. ARCE, *Thin Solid Films* **204** (1991) 405.
16. R. ASOMOZA, A. MALDONADO, J. RICKARDS, E. P. ZIRONI, M. H. FARIAS, I. COTA-ARAIZA and G. SOTO, *ibid.* **203** (1991) 195.
17. M. MIKI-YOSHIDA and E. ANDRADE, *ibid.* **224** (1993) 87.
18. T. KARLSSON, A. ROOS and C. G. RIBBING, *Solar Energy Mater.* **11** (1985) 469.
19. C. AGASHE, M. G. TAKWALE, B. R. MARATHE and V. G. BHIDE, *ibid.* **17** (1988) 99.
20. N. SRINIVASA MURTY and S. R. JAWALEKAR, *Thin Solid Films* **100** (1983) 219.
21. K. ADACHI and M. MIZUHASHI, in "Chemical Vapor Deposition", edited by G. W. Cullen and J. M. Blocher Jr., PV 87-8 (Electrochemical Society Softbound, Proceedings Series, Pennington, NJ, 1987) p. 999.
22. C. A. VINCENT, *J. Electrochem. Soc.* **119** (1972) 515.
23. A. F. CAROLL and L. H. SLACK, *ibid.* **123** (1976) 1889.
24. E. SHANTHI, V. DUTTA, A. BANERJEE and K. L. CHOPRA, *J. Appl. Phys.* **51** (1980) 6243.
25. J. BRUNEAUX, H. CACHET, M. FROMENT and A. MESSAD, *Thin Solid Films* **197** (1991) 129.
26. R. C. WEAST (ed.), "Handbook of Physical Chemistry", 63rd Ed. (CRC Press, Boca Roton, USA, 1982).
27. D. R. PYKE, R. REID and R. J. D. TILLEY, *J.C.S. Farad. I* **76** (1980) 1174.
28. J. GALY, G. MEUNIER, S. ANDERSON and A. AASTROM, *J. Solid State Chem.* **13** (1975) 142.
29. D. PYKE, R. REID and R. J. D. TILLEY, *ibid.* **25** (1975) 142.
30. G. W. GODIN, C. C. McCAIN and E. A. PORTER, in "Proceedings of the IV International Congress on Catalysis", Moscow (1968) Vol. 1 (Akadimiai Kindó, Budapest, 1971) p. 271.
31. K. WAKABAYASHI, Y. KAMIYA and H. OHTA, *Bull. Chem. Soc. Jpn* **40** (1967) 2172.
32. E. GERLACH and P. GROSSE, *Festkörperprobleme* **17** (1977) 157.
33. Z. M. JARZEBSKI and J. P. MARTON, *J. Electrochem. Soc.* **123** (1976) 199C.
34. G. SANON, R. RUP and A. MANSINGH, *Phys. Status Solidi* **A135** (1993) 581.
35. J. LINDHARD, *Kgl. Danske Videnskab. Selskab., Mat.-Fgs. Medd.* No. 8 (1954) 28.
36. D. PINES, "Elementary excitations in solids" (Benjamin, New York, 1964) p. 126–44.
37. B. DUKE, "Solid State Physics", Suppl. 10 (Academic Press, New York, 1969) p. 60.

Received 22 June 1993
and accepted 21 March 1994